euspen's 21st International Conference & Exhibition, Copenhagen, DK, June 2021
www.euspen.eu

5-Axis ultra-precision diamond shaping of blazed diffraction gratings on high curvature convex ellipsoidal surfaces

Nicholas Yew Jin Tan[1,2], A Senthil Kumar[1], Guangya Zhou[1], Kui Liu[2]

[1]*Department of Mechanical Engineering, National University of Singapore, 10 Kent Ridge Crescent, 9 Engineering Drive 1, Block EA, Singapore 117576, Singapore*
[2]*Singapore Institute of Manufacturing Technology, 71 Nanyang Drive, Singapore 638075, Singapore*

Email: ntan9792@gmail.com

Abstract
As the requirements for functional optical profiles transcend their regular forms, traditional manufacturing techniques begin to prove to be insufficient in producing such features due to the lack of axial flexibility. This is especially apparent in the fabrication of freeform blazed optical gratings used for diffraction in spectroscopy. The challenge arises when attempting to maintain the tool rake angle constant along the desired surface, avoiding geometrical inaccuracies caused by such change. On higher curvature gratings, these discrepancies become extremely pronounced. Thus, a new 5-axis Continuous Rotating Freeform Shaping (CRFS) algorithm is proposed in this paper to fabricate new freeform diffraction gratings, which was previously unattainable using conventional techniques. By compensating the linear deviations required to maintain rake angle along the surface and positioning the tool flank to shape the blazed angles across the surface, these gratings can be easily achieved by fully utilizing all 5-axes using synchronized slow slide servo movement. In this study, blazed gratings were successfully machined on a brass workpiece with an ellipsoidal form using a 5-axis ultra-precision machine.

Ultra-precision, Diamond, Micromachining, Optical

1. Introduction

The constant search for more compact yet functional devices have often led to complex component designs. This has not spared optical structures, requiring more convoluted forms to extract ever more performance potential. Coupled with stringent requirements required by the optical industry, conventional production techniques have begun to become inadequate to develop these complex freeform structures.

This evolution in form complexity can be observed in development of reflective diffraction gratings, especially those used for spectroscopy. Such spectrometers have seen a wide application in various industries, including and not limited to biomedicine [1], environmental studies [2] and astronomy [3,4]. Traditionally, gratings on flat plane surfaces are used to split the various wavelengths of light. These plane gratings can be easily produced with relative efficiency using specialized devices called ruling engines [5]. However, such machines have little production flexibility, locking precious capital investment into a single product line.

Thus, researchers begin exploring the use of compounded optical components. These components serve more than one function, reducing the overall number of components required and in turn, the footprint of the device. As such, the use of gratings with concave or convex forms are increasing in relevancy, replacing the use of the conventional plane gratings. These new forms reduce the overall reliance on lenses and mirrors, lowering the overall production cost of the device. The removal of the lenses also allows for better UV and IR performance as such wavelengths would otherwise be absorbed by the lens material, and where alternative lens materials would drive up the overall cost.

Nevertheless, direct fabrication of such features has shown to be very challenging due to the complexity of the form. Researchers have worked around this by developing other grating techniques like holographic grating patterning using dual-beam interference lithography [6]. This is done by coating a photoresist over a polished substrate and exposing the standing wave pattern of the two laser beams. This results in straight gratings which can be projected on freeform surfaces using the appropriate lenses. However, the grooves produced by this technique possess a sinusoidal profile, which has shown to be considerably less efficient compared to its blazed counterparts [7].

On the other hand, ruling engines face difficulty in producing blazed gratings in such forms. Thus, a machine with more axial flexibility is required. Ultra-Precision Machine (UPM) fits the bill as it is not only able to do optical gratings, albeit more slowly, but also many other optical components. Using diamond tools, such optical components can be directly produced with little need for post processing due to the excellent geometrical accuracy and mirror-like surface finish.

As such, ultra-precision diamond shaping (UPDS) using a 5-axis UPM is proposed, along with the Continuous Rotating Freeform Shaping (CRFS) algorithm, to produce these freeform gratings. UPDS has shown to be extremely flexible in producing unique and unconventional features by employing the use of the machine's slow slide servo, while the CRFS algorithm allows for a constant rake along the surface and compensates for the translational deviations [8,9].

In this paper, the development of the CRFS algorithm is discussed, along with the experimental results and analysis of the high curvature ellipsoidal demonstrator.

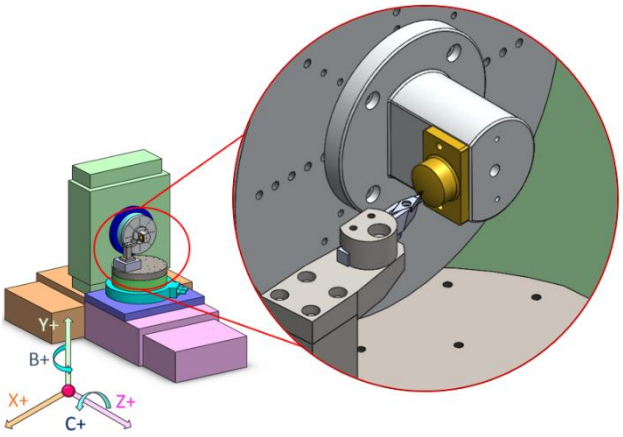

Figure 1. 5-axis freeform blazed grating set-up.

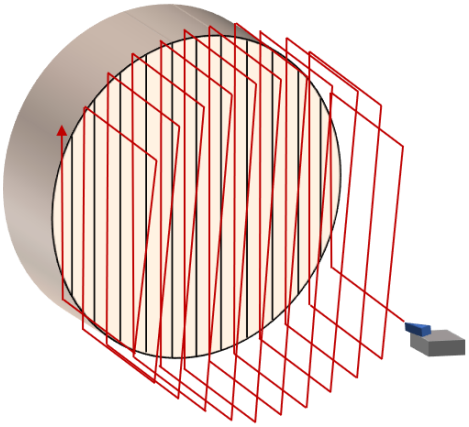

Figure 2. Conventional shaping technique for gratings on the UPM.

2. Continuous Rotating Freeform Shaping

UPDS of freeform blazed gratings requires the use of the CFRS algorithm. This encompasses the generation of the 3D surface profile along the direction of the gratings, the algorithmic rake angle compensation to conform to the surface and orientating the tool flank to shape the functional face of the groove at the desired angle. The following sections will discuss these in detail.

2.1. Ellipsoidal surface generation

Before the surface can be generated, it is important that the surface of interest is aligned accordingly as in Figure 1. This is to avoid complications with the orientation of the surface when manipulated. As a parallel turning setup is employed, the surface of interest is to be positioned at the 9 o'clock location with the surface away from the spindle axis, while the gratings are aligned top-down. This setup allows for high curvature gratings which can significantly reduce the overall spectrometer size.

As with all surfaces, 3D Cartesian equations (*x, y, z*) can be used to define the profile of interest. A triaxial ellipsoidal surface was selected as a demonstrator for the 5-axis UPDS algorithm. This surface can thus be defined as follows:

$$\frac{x^2}{a^2}+\frac{y^2}{b^2}+\frac{z^2}{c^2}=1 \tag{1}$$

Where *a, b* and *c* are constants of the principle semiaxes corresponding to *x, y* and *z* respectively. The zeros of the *X*- and *Y*- axis were set to the spindle centre and the *Z*- axis zero was set to the centre of the workpiece. To avoid convolution, the equation can be reduced to two variables by including the size of the grating, usually given from the inverse of the grating density. For this demonstrator, *a, b,* and *c* were set at 70, 40 and 50 mm respectively. The line density selected was at 80 lines per mm, giving a grating width of 12.5 µm. To align the surface of the workpiece to the surface, *x* in eqn (1) is substituted as follows:

$$x \rightarrow x_R = x - x_c \tag{2}$$

Where x_c is the offset distance of the feature centre from the spindle axis, which is set at 40mm. This aligns the surface to a workpiece set at a radius of 30 mm away from the spindle axis.

With the position of the grating lines determined, the equation of each section profile is obtained. Here, the point cloud of the surface can be generated according to the grating lines. To maintain a constant local speed across the profile, the point distance, d, must be fixed. This was set at 0.1 mm and the point cloud can be obtained as follows:

$$\sqrt{(x-x_1)^2+(y-y_1)^2}=d \tag{3}$$

Where x_1 and y_1 are the *x* and *y* coordinates of the previous reference point. This reference point can be set at *y* = 0, giving an *x* value as a starting reference. By iterative solving of eqn (1) and eqn (3), the points for each sectional profile can be generated in terms of X and Y. This must only be done for the section of the profile reflected on the surface of the workpiece. For this experiment, the surface of interest has a radius of 10 mm. The minimum and maximum y value of the feature can thus be determined by the following equation based on a circular surface:

$$\pm y = \sqrt{r^2-d^2} \quad (d = +z \rightarrow -z) \tag{4}$$

Where r is the radius of the feature and *d* is the distance of the profile of interest from the *Z* origin. This is determined from y- to y+, creating an upward moving shaping path. Thus, the surface point cloud is ready for conversion for 5-axis UPDS.

2.2. Rake angle compensation

In traditional shaping of features, the point cloud given in section 2.1 is sufficient to generate the surface. This is usually done by aligning the tool to the grating location before moving in the tool to the desired depth and shaping out the grating from bottom-up, as seen in Figure 2. However, this process has several flaws. Firstly, gratings produced by this technique are very inefficient due to repeated acceleration and deceleration required to position each line moving from point-to-point. Also, as the tool is indexing, there are some minor depth discrepancies due to positioning errors between each grating pass, affecting the overall quality of the grating. Furthermore, highly curved surfaces pose a challenge due to the varying rake angles across the surface, as well as insufficient front clearance. The change in rake angle leads to variation in the amount of material removed due to change in the contact interface, while the collision with the front clearance will inevitably damage the desired feature.

Thus, synchronized 5-axis UPDS provides the axial flexibility required to fabricate such gratings on highly curved surfaces, while the CRFS algorithm complements it and increases the flexibility of the UPM to generate freeforms.

The CRFS algorithm works by firstly allocating each point to an angle based on the position of the point to the spindle axis. This is done for each profile of Z, allowing the point locale angle, ϑ_R to be obtained as follows:

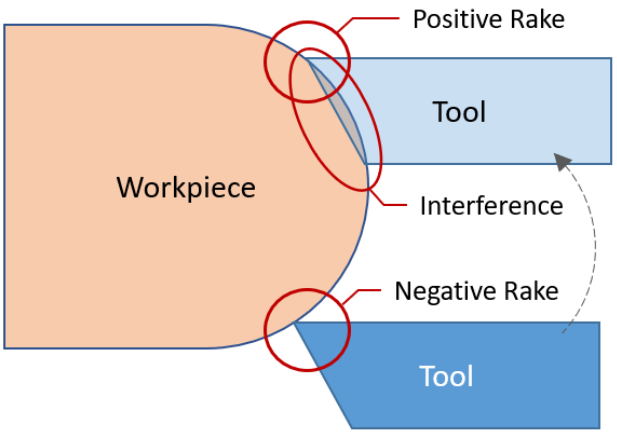

Figure 3. Cross-sectional view on the challenges faced by conventional grating techniques on high curvature features

$$\vartheta_R = \text{atan}\frac{y}{x} \tag{5}$$

Where *x* and *y* are each of the surface coordinates derived from eqn (1) and eqn (3). However, ϑ_R cannot be directly converted into the C-coordinates required for developing the surface using the slow slide servo. Due to the uneven topology of the component, the rake angle of the tool varies from point-to-point. Thus, using these coordinates will still lead to unintended deviations in terms of tool-workpiece contact front. As such, the next part of the CRFS algorithm is required, aligning the tool with zero rake to the surface, as well as compensating the translational deviations in both the X and Y directions.

To obtain the rake angles required, the gradient of the slope of each point must be determined. However, due to convolution of the surficial variable, these values cannot be directly extracted by the derivative of the *XY* sliced profiles with respect to Z. This may result in implicit equations with imaginary roots. Thus, a more encompassing approach is required, allowing for any profile form.

As the distance between every point was derived to be of fixed length using the profile equation, a two-point gradient approximation (2PGA) can be used instead of the derivative. The gradient of each point, ϑ_m, is thus determined as follows:

$$(\vartheta_m)_{2\leq i\leq n-1} = \text{atan}\frac{y_{i-1} - y_{i+1}}{x_{i-1} - x_{i+1}} \tag{6}$$

By obtaining the gradient of the point, ϑ_m can be directly translated into the C-coordinates used for CRFS as it aligns with a zero-rake angle to the freeform surface. However, due to the mismatch in the positions of both ϑ_R and ϑ_m, compensation of the linear deviations is required. This must be taken with respect to each point, as seen in Figure 4. As such, the XYZC coordinates can be determined as follows:

$$R = \sqrt{x^2 + y^2} \tag{7}$$

$$\varphi = 90 - \vartheta_m \tag{8}$$

$$S = 2\left[R\,sin\left(\frac{\varphi}{2}\right)\right] \tag{9}$$

$$\rho = \left[\frac{(180 + \varphi)}{2} + \vartheta_R\right] - 90 \tag{10}$$

$$Y = y - S\cos(\rho) \tag{11}$$

$$X = x + S\sin(\rho) \tag{12}$$

Where R is the distance of the point from the spindle axis located at (X_0, Y_0), φ is the angle of rotation required to align the rake angle, *S* is the length of the sector between the spindle axis and the shifted origin (X'_0, Y'_0), while ρ is the direction of the sector in respect with the Y plane. The machine coordinates for each point of interest can then be determined at point (X, Y), compensated for the rotation of the spindle.

2.3. Grating alignment

Once the surface can be generated, the final feature required to be shaped is the blaze angle of the gratings. For this demonstrator, the blaze angle is fixed at 8.25° from the tangent of the surface. By extracting the XZ profile of the surface at Y=0, the tangents of the profile can easily be extracted by its derivative or using the 2PGA method as described in eqn (6).

Once all the B coordinates are determined, the last step is to create a continuous path for the machine. This crucial step allows for smooth transitions without accelerations and decelerations between each grating, significantly speeding up the process using block processing. Once the tool leaves the grating surface, virtual points are allocated in all 5 axes. The values of the *XYZBC* coordinates are spaced equally from the end of one line to the start of the next, creating a smooth transition. This thus creates a continuous spiral, with the position of the linear grating lines at the profile of interest. As such, the ellipsoidal constant-angle blazed gratings can be machined.

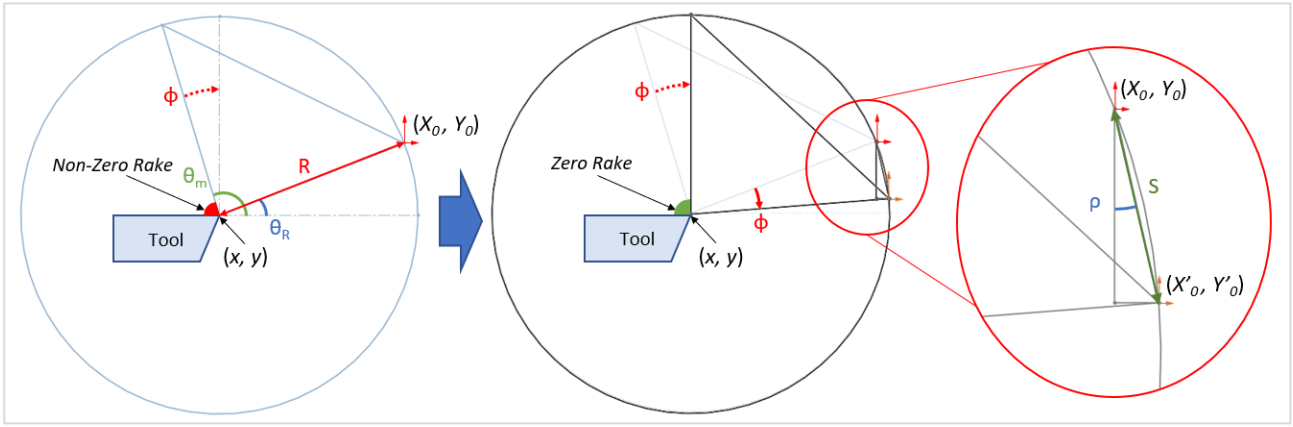

Figure 4. CRFS schematic for obtaining the compensated X and Y values to compensate for the rake angle deviations. The coordinate of interest is at point (x, y), while its origin locale is shifted to point (X'_0, Y'_0).

3. Experimental Verification

To verify the CFRS algorithm, the process was conducted in a 5-axis UPM. The physical setup to execute the shaping process is presented in Figure 5. A brass workpiece with a cylindrical diameter of 10 mm was affixed to the spindle. To reduce noise and vibrations caused by an unbalanced spindle, dynamic balancing and compensation were conducted during the set-up process.

A conventional 35-degree included angle sharp diamond tool was used to fabricate the demonstrator, with a front clearance of 15 degrees. Using a 50x telecentric camera, the tip of the tool was aligned with the B- stage axis of rotation, allowing the gratings to be formed without the need to compensate for geometrical run-outs due to axial misalignment.

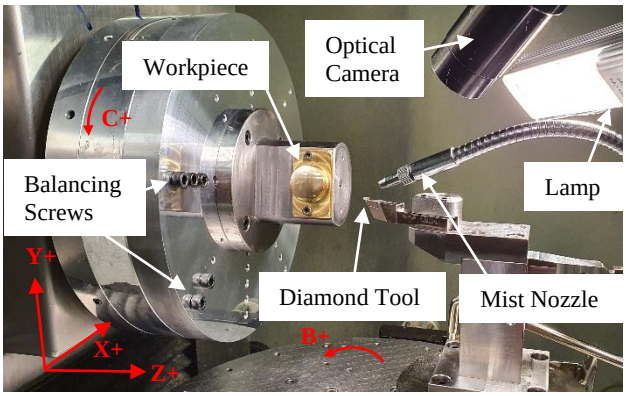

Figure 5. Experimental set-up for CRFS. The tip of the tool was aligned with the centre of the B-stage for ease of shaping.

4. Results and Discussion

Using the CRFS algorithm, the ellipsoidal gratings were successfully machined on the surface of the brass workpiece, as shown in Figure 6. The quality of the machining process was measured using a laser confocal microscope. The surface roughness of the workpiece was measured with an Ra of 6 nm on the blazed surface. This corroborates well with the exceptional surface finishing of ultra-precision products using diamond shaping.

The profile of the lens was also measured across the lens and from top-down, intersecting with the lens apex at 10X zoom. Due to the complexity of the shape, the curvature of the structure was measured instead. This was measured to be 23.664 mm on the XY plane and 36.072 mm along the XZ plane, deviating from the designed curvature by 0.084% and 0.017% respectively. Using the cross-section of the gratings, the blazed angles were measured with a deviation of ±0.01 degree and the grating size was measured with an average of 12.5075 µm with an optical zoom of 50X.

Hence, with the successful shaping of the triaxial ellipsoidal gratings, the CRFS algorithm has displayed its viability in the production of high-quality blazed gratings on freeform surfaces, even with high curvatures. This allows for the ease of fabrication for future freeform reflective gratings, allowing for higher resolution applications, especially in spectroscopy.

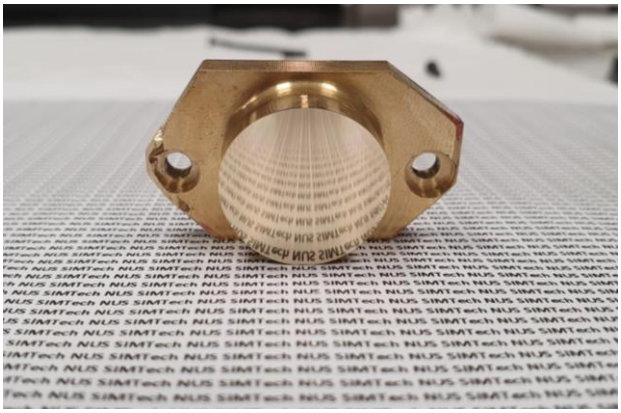

Figure 6. The blazed gratings were successfully machined upon the ellipsoidal surface of a brass workpiece using the developed CRFS algorithm.

5. Conclusion

The blazed gratings were successfully machined on a high curvature triaxial ellipsoidal surface of a brass workpiece. This was done using a UPDS technique which employs three translational axes and two rotational axes, namely the X-, Y-, Z-, B- and C- axes. The CFRS algorithm developed in this paper converts the XYZ 3D point cloud into coordinates of which allows the UPM to produce the optical surface with a surface finish of 6 nm.

The CFRS algorithm maintains the rake angle of the tool along the freeform surface by positioning the spindle at the corresponding rake angle of the point of interest while compensating for the deviations translationally to maintain the tool workpiece interaction. This allows for the fabrication of the blazed gratings on freeform surfaces. The use of the slow-slide servo also allows for the process to be repeated reliably, and for multiple passes with little to no mismatch of the tool tip between passes.

Hence, freeform blazed gratings can now be fabricated on the UPM with exceptional quality and are now no longer limited by the shape of the lens. This enables the development of more complex optical designs, advancing optoelectronic and photonic applications.

References

[1] Naumann D 2011 FT-Infrared and FT-Raman Spectroscopy In Biomedical Research *Appl. Spectrosc. Rev.* ***36*** *239-98*

[2] Shi T, Guo L, Chen Y, Wang W, Shi Z, Li Q, Wu G 2018 Proximal and remote sensing techniques for mapping of soil contamination with heavy metals *Appl. Spectrosc. Rev.* ***53*** *783-805*

[3] Saito S 2006 Laboratory Microwave Spectroscopy of Interstellar Molecules *Appl. Spectrosc. Rev.* ***25*** *261-296*

[4] Oertel GK and Epstein GL 2007 Current Solar Spectroscopic Research *Appl. Spectrosc. Rev.* ***10*** *139-200*

[5] Mi X, Zhang S, Qi X, Yu H, Yu H, Tang Y 2019 Ruling engine using adjustable diamond and interferometric control for high-quality gratings and large echelles *Opt. Express* **27** 19448-62

[6] Li X, Ni K, Zhou Q, Wang X, Tain R, Pang J 2016 Fabrication of a concave grating with a large line spacing via a novel dual-beam interference lithography method *Opt. Express* **24** 10759 -66

[7] Breidne M, Johansson S, Nilsson L-E, Åhlèn H 1979 Blazed Holographic Gratings *Op*t. Acta: Int. J. Opt. 26 1427-41

[8] Tan NYJ, Zhang X, Neo DWK, Liu K, Kumar AS 2019 Ultra-precision diamond shaping of microchannels for microfluidic applications *euspen's 19th Int. Conf. Exhibit., Bilbao, Spain.* 358-61

[9] Tan NYJ, Ng YH, AS Kumar, Liu K 2020 Ultra-precision direct diamond shaping of composite polygonal Fresnel lenses *euspen's 20th Int. Conf. Exhibit., Geneva, Switzerland.* 381-4